AD-A170 946 METALLURGICAL VARIABLES INFLUENCING THE CORROSION SUSCEPTIBILITY OF P/M (..(U) NAVAL AIR DEVELOPMENT CENTER WARMINSTER PA AIRCRAFT AND CREW S.. 1/1

UNCLASSIFIED R C PACIEJ ET AL. 01 OCT 85 NADC-86071-60 F/G 11/6 NL

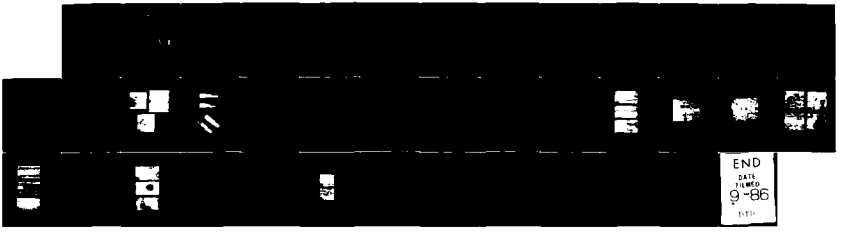

END
DATE FILMED
9-86
DTIC

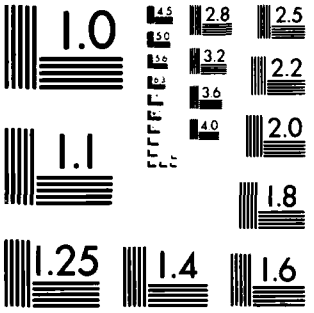

MICROCOPY RESOLUTION TEST CHART
NATIONAL BUREAU OF STANDARDS-1963-A

REPORT NO. NADC-86071-60

(12)

AD-A170 946

METALLURGICAL VARIABLES INFLUENCING THE CORROSION SUSCEPTIBILITY OF P/M 7091 ALUMINUM/SiCw COMPOSITE

R. C. Paciej and V. S. Agarwala
Aircraft and Crew Systems Technology Directorate
NAVAL AIR DEVELOPMENT CENTER
Warminster, Pennsylvania 18974-5000

DTIC
ELECTE
AUG 1 8 1986
S D
D

OCTOBER 1985

FINAL REPORT
P.E. 62761N

Approved for Public Release: Distribution Unlimited.

DTIC FILE COPY

Prepared for
NAVAL AIR SYSTEMS COMMAND
Department of the Navy
Washington, DC 20361

86 8 18 032

NOTICES

REPORT NUMBERING SYSTEM — The numbering of technical project reports issued by the Naval Air Development Center is arranged for specific identification purposes. Each number consists of the Center acronym, the calendar year in which the number was assigned, the sequence number of the report within the specific calendar year, and the official 2-digit correspondence code of the Command Office or the Functional Directorate responsible for the report. For example: Report No. NADC-78015-20 indicates the fifteenth Center report for the year 1978, and prepared by the Systems Directorate. The numerical codes are as follows:

CODE	OFFICE OR DIRECTORATE
00	Commander, Naval Air Development Center
01	Technical Director, Naval Air Development Center
02	Comptroller
10	Directorate Command Projects
20	Systems Directorate
30	Sensors & Avionics Technology Directorate
40	Communication & Navigation Technology Directorate
50	Software Computer Directorate
60	Aircraft & Crew Systems Technology Directorate
70	Planning Assessment Resources
80	Engineering Support Group

PRODUCT ENDORSEMENT — The discussion or instructions concerning commercial products herein do not constitute an endorsement by the Government nor do they convey or imply the license or right to use such products.

APPROVED BY:  DATE: 21 April 1986

UNCLASSIFIED

SECURITY CLASSIFICATION OF THIS PAGE AD-A170946

REPORT DOCUMENTATION PAGE

1a REPORT SECURITY CLASSIFICATION Unclassified	1b RESTRICTIVE MARKINGS
2a SECURITY CLASSIFICATION AUTHORITY	3 DISTRIBUTION/AVAILABILITY OF REPORT Approved for Public Release; Distribution Unlimited
2b DECLASSIFICATION/DOWNGRADING SCHEDULE	
4 PERFORMING ORGANIZATION REPORT NUMBER(S) Report No. NADC-86071-60	5 MONITORING ORGANIZATION REPORT NUMBER(S) N/A
6a NAME OF PERFORMING ORGANIZATION Naval Air Development Center Aircraft & Crew Systems Dir.	6b OFFICE SYMBOL (If applicable) 6062
7a NAME OF MONITORING ORGANIZATION N/A	
6c ADDRESS (City, State, and ZIP Code) Warminster, Pennsylvania 18974-5000	7b ADDRESS (City, State, and ZIP Code) N/A
8a NAME OF FUNDING/SPONSORING ORGANIZATION Naval Air Systems Command	8b OFFICE SYMBOL (If applicable)
9 PROCUREMENT INSTRUMENT IDENTIFICATION NUMBER	
8c ADDRESS (City, State, and ZIP Code) Washington, DC 20361	10 SOURCE OF FUNDING NUMBERS PROGRAM ELEMENT NO: PE 62761N; PROJECT NO; TASK NO; WORK UNIT ACCESSION NO

11 TITLE (Include Security Classification)

Metallurgical Variable Influencing the Corrosion Susceptibility of P/M 7091 Aluminum/SiCw Composite

12 PERSONAL AUTHOR(S)
Paciej, Richard C. and Agarwala, Vinod S.

13a TYPE OF REPORT	13b TIME COVERED	14 DATE OF REPORT (Year, Month, Day)	15 PAGE COUNT
Final	FROM _____ TO _____	1 Oct 1985	

16 SUPPLEMENTARY NOTATION

17 COSATI CODES		
FIELD	GROUP	SUB-GROUP

18 SUBJECT TERMS (Continue on reverse if necessary and identify by block number)
Metallurgical Variables; Susceptibility
Corrosion; P/M 7091 Aluminum/SiCw Composite

19 ABSTRACT (Continue on reverse if necessary and identify by block number)

Corrosion studies of a 20 v/o SiCw/P/M 7091 aluminum composite material were performed. The plate material which was heat treated to the T-6 and T-7 temper by conventional methods, showed preferential corrosion of the surface layers up to 2 mm thick. The regions of corrosion susceptibility were determined to be due to improper processing and thermal treatments. Cold worked regions due to extrusion were not completely removed by the conventional solution treatment and thus appeared as more corrosion susceptible. Large void volume fraction and excessive segregation of SiCw was also noted. Electrochemical, microscopic and analytical techniques were used in these investigations. Attempts were made to remove the cold worked regions and study the resultant corrosion properties. A comparative analysis of these results is discussed.

20 DISTRIBUTION/AVAILABILITY OF ABSTRACT	21 ABSTRACT SECURITY CLASSIFICATION
☐ UNCLASSIFIED/UNLIMITED ☒ SAME AS RPT ☐ DTIC USERS	Unclassified
22a NAME OF RESPONSIBLE INDIVIDUAL R.C. Paciej	22b TELEPHONE (Include Area Code) / 22c OFFICE SYMBOL 6062

DD FORM 1473, 84 MAR 83 APR edition may be used until exhausted
All other editions are obsolete

SECURITY CLASSIFICATION OF THIS PAGE

UNCLASSIFIED

A

TABLE OF CONTENTS

	Page
INTRODUCTION	1
EXPERIMENTAL PROCEDURE	2
Materials	2
Corrosion Studies	2
Electrochemical Studies	2
Microstructural Studies	6
Elemental Analysis	6
Hardness Measurements	6
Density Measurements	6
RESULTS AND DISCUSSION	7
Corrosion Studies	7
Electrochemical Studies	10
Scanning Electron and Optical Microscopy	15
EDAX, DSC and X-Ray Analysis	21
Elemental Analysis	21
Hardness Tests	23
Density Measurements	23
CONCLUSIONS	26
REFERENCES	27

Accesion For
NTIS CRA&I ☒
DTIC TAB ☐
Unannounced ☐
Justification .....
By .....
Dist ibution /
Availability Codes
Dist | Avail and / or Special
A-1

DTIC COPY INSPECTED 1

LIST OF TABLES

Table		Page
1	Elemental Compositions of the Material in w/o.	3
2	Heat Treatments for P/M Al/SiCw Composite and MA-87 Al Alloy	5
3	Typical Corrosion Potential, Polarization Resistance and Potentiodynamic Test Results.	14

LIST OF FIGURES

Figure		Page
1	A typical flow chart depicting production sequence for an extruded P/M metal matrix composite (5)	4
2	Photographs showing the preferential attack of the A(T6) P/M 7091 Al/SiCw composite in aerated 3.5% NaCl, pH 6: (A) specimen after total immersion for 3 days; (B) transverse face of a machine-finished specimen polished and etched showing residual work hardening effects; (C) Rockwell B indentation in the core region with plastic zone corroded	8
3	Exfoliation test specimens; (A) short transverse face, (B) short transverse and longitudinal faces	9
4	Galvanic current density/time plots of (A) A(T6) specimen versus MA-87 alloy and (B) skin versus core regions of A(T6) specimen in aerated 1.0% NaCl, pH 2	11
5	Corrosion potential versus time plots for; (A) A(T6), (B) MA-87, (C) and (D), the core and skin regions of the A(T6) in deaerated 3.5% NaCl, pH 6	12
6	Potentiodynamic polarization behavior of the composite: (A) A(T6) specimen, (B) skin and (C) core regions of specimen A(T6) in deaerated 3.5% NaCl, pH 6	13
7	Optical micrographs of the A(T6) specimen's (A) skin region before testing, (B) skin region and (C) core region after polarization at -0.69V. Magnification 200x	16
8	Scanning electron micrograph of the A(T6) specimen's core region etched with Kellers reagent. Magnification 400x	17
9	Optical micrograph of the A(T6) specimen's skin region etched with Keller's reagent showing foreign particles not broken-up by the extrusion process. Magnification 800x	18
10	Scanning electron micrographs of the A(T6) specimen's skin region at (A) 1000x and (B) 520x; and core region at (C) 2000x and (D) 1000x after the total immersion in aerated 3.5% NaCl, pH 2	19
11	Optical micrographs of the A(T6) specimen's (A) skin region, (B) core region; and (C) core region of the G(T6) specimen after total immersion in aerated 1% NaCl, pH 6 for three hours. Magnification 800x.	20
12	(A) Scanning electron micrograph of the A(T6) specimen electrochemically etched at -0.69V in deaerated 1% NaCl, pH 2 for 10 minutes; (B) and (C) are the X-ray mappings for zinc and copper, respectively, for figure (A). Magnification 5000x	22

LIST OF FIGURES (Continued)

Figure		Page
13	Profile of the Knoop microhardness values across the composite plate thickness	24
14	Scanning electron micrographs of the A(T6) specimen's (A) skin and (B) core regions. Final polished to 0.05 μm Al 0. Magnification 1200x	25

INTRODUCTION

The incorporation of SiC whiskers (SiCw) into a metal matrix has increased the interest for these materials (1). SiC whiskers made from rice hulls are potentially low in cost and can be easily incorporated into Al and Mg alloy matrices using powder metallurgy (P/M) technology. Metal matrix composites (MMC) reinforced with discontinuous fibers, are isotropic, have the advantage of versatility in fabrication, and have strength levels which are equivalent or superior to the best heat treatable Al alloys. The stiffness of these composites ranges from 1 to 3.5 times that of conventional Al alloys. However, the strain to failure for the MMC is only 1.5% due to its low ductility (2). The major concerns with MMC are that they are heterogeneous and the material property data are relatively sparse.

SiCw/Al alloy composite fabrication processes have inherent problems. One of them is the blending of prealloyed Al powder with SiC whiskers (3, 4, 5). The whisker surfaces may become flawed during blending and their intrinsic, as-produced properties and aspect ratios can be reduced. The extrusion of the SiCw-containing composite billets can cause additional damage to the whiskers (3, 6). In early MMC, a very poor homogeneity of the SiCw reinforcement was found (4, 5, 7). They also contained voids and small scale porosity. More recently, improvements in the ductility and homogeneity of SiCw/Al alloy composites have been made by using much larger billets (larger than 6 inches in diameter) which results in a greater reduction ratio during extrusion (7). The effect of using a larger reduction ratio is to decrease matrix porosity and reduce the size of inclusions. The possibility of introducing contaminants to the powder is also a problem (5, 7).

Thermal problems may also have a detrimental effect on the properties of MMC. Heat treatments for SiC/Al alloy MMC may have to be different than the conventional heat treatments for the matrix materials. New heat treatments may be required because, both the SiCw and Al alloy matrix possess vastly different thermal properties. This difference may result in a situation of a high residual stress and a high dislocation density at the SiCw-Al alloy interface after subsequent heat treating cycles (8).

The corrosion behavior of SiCw/Al alloy MMC has only recently been studied (1, 9, 10, 11). DeJarnette and Crowe (1) compared 20v/o SiC/2024 Al with commercially extruded 20241A1-T4 in deaerated 3.5% NaCl solution and found that the corrosion rates were similar. In aerated solutions the corrosion rate was 40% higher for the composite in a four-week exposure test. Wolf et al. (11) found little difference in corrosion rates in 3.5% NaCl solution when the SiCw volume was increased from 0 to 30v/o for a SiC/6061 Al composite. McCafferty and Trzaskoma (9) found a lower pitting potential for a SiC/2024 Al composite as compared to the wrought matrix. In general, MMC can become more corrosion susceptible due to (1) galvanic coupling – the reinforcing phase or the interface reaction layer may act as a cathode; (2) selective corrosion in the interfacial region or from crevice corrosion when there are gaps in the interfacial region; and (3) matrix defects. The corrosion property data on MMC is sparse in the literature.

The initial purpose of this study was to investigate the corrosion behavior of an extruded P/M 7091A1-20v/o SiCw composite plate. However, it was found that the plate exhibited an abnormal corrosion behavior. The composite plate's exterior (skin area) was observed to corrode preferentially. Thus, it was of interest to determine the nature and cause of this phenomenon. Electrochemical, microscopic, and analytical techniques were employed in the investigations. Various solution heat treatment times and temperatures were used to eliminate the preferential attack of the composite's skin.

EXPERIMENTAL PROCEDURE

MATERIALS

The materials used for this study were Alcoa MA-87 alloy and P/M 7091A1-20v/o SiCw (Arco Metal Co.) composite. The nominal compositions of the Al prealloyed powder material and the MA-87 alloy are listed in Table 1. The SiCw reinforcement was made from rice hulls. A flow chart depicting the production sequence of the composite is shown in Figure 1. The extruded plate dimensions were 36x5x0.5 inches. It was produced from a 6 inch diameter billet. The composite materials used for testing were previously conventionally heat treated to the T6 and T7 conditions. Subsequent solution heat treatment times and temperatures for all specimens used are listed in Table 2. The extruded MA-87 alloy was stress relieved by stretching and heat treated to the T7E69 condition.

CORROSION STUDIES

The general corrosion behavior of the A(T6) composite material (listed in Table 1) and the MA-87 alloy were determined by measuring the weight change after total immersion tests in 3.5% NaCl solutions of pH 2 and 6. Specimens were exposed in the solution for three days and then cleaned in 50v/o nitric acid. Exfoliation tests were performed on stepped specimens in accordance with the ASTM Standard Method G34-79(12). The stepped specimens were machined to expose the T/2, T/10 and the top layer. Composite materials A(T6) and G(T6) listed in Table 2 were used for this test. Materials C(T6), D(T6), E(T6) and F(T6) were used for total immersion tests in 3.5% NaCl (pH 2) to observe the effect of varying solution heat treatment times and temperatures on the preferential attack of the composite's skin region.

ELECTROCHEMICAL STUDIES

The experimental program consisted of examining the electrochemical behavior of the composite as a whole and of the separated skin and core regions. Thus, a sample was chosen which consisted of a large skin region. Potentiodynamic polarization measurements were made on the A(T6) material. Steady-state open circuit potentials (corrosion potentials), polarization resistances, corrosion current densities and anodic and cathodic tafel slopes were determined. The test media was a 3.5% NaCl solution. Solutions were purged with argon at least one hour before the start of the experiments unless otherwise indicated. All specimens were cold-mounted in epoxy with their (S-L) face open for exposure. They were used for potentiodynamic polarization, galvanic (couple) corrosion and controlled potential corrosion tests. The galvanic couples were: (1) A(T6) material versus MA-87 alloy; and (2) skin versus core of A(T6) material. All couples had 1:1 exposed surface area. The exposed surfaces of all test specimens were polished using standard metallographic techniques and finished to 1000 grit.

For the galvanic couple tests, the current between the two specimens (electrodes) was measured using a zero-resistance ammeter and recorded as a function of time. The test was done in aerated 1% NaCl (pH 2) solution.

For the polarization measurements, a potential range of -1.2 to -0.55 volts was selected at a scan rate of 0.166 mV/sec. Generally, before the start of the polarization experiments, both the steady-state open circuit (corrosion) potential and polarization resistance measurements were made. In some cases, after solution purging, the potential scan was started as soon as the specimen was placed into the test solution. The results were most reproducible when the latter technique

TABLE 1

ELEMENTAL COMPOSITIONS OF THE MATERIAL IN W/O

Material	Cu	Mn	Mg	Si	Cr	Fe	Zn	Ti	Co	Al
Prealloyed SXA 7091 powder	1.58	t	2.40	t	t	0.07	6.10	0.05	0.40	89.4
7091 Al/SiC_w composite										
a) Skin	1.64	t	2.88	0.54	t	0.73	5.32	t	0.33	88.6
b) Core	1.65	t	2.63	0.64	t	0.38	5.38	t	0.37	88.9
MA-87	1.50	-	2.50	-	0.10	0.10	6.50	-	0.40	89.9

t- trace quantity

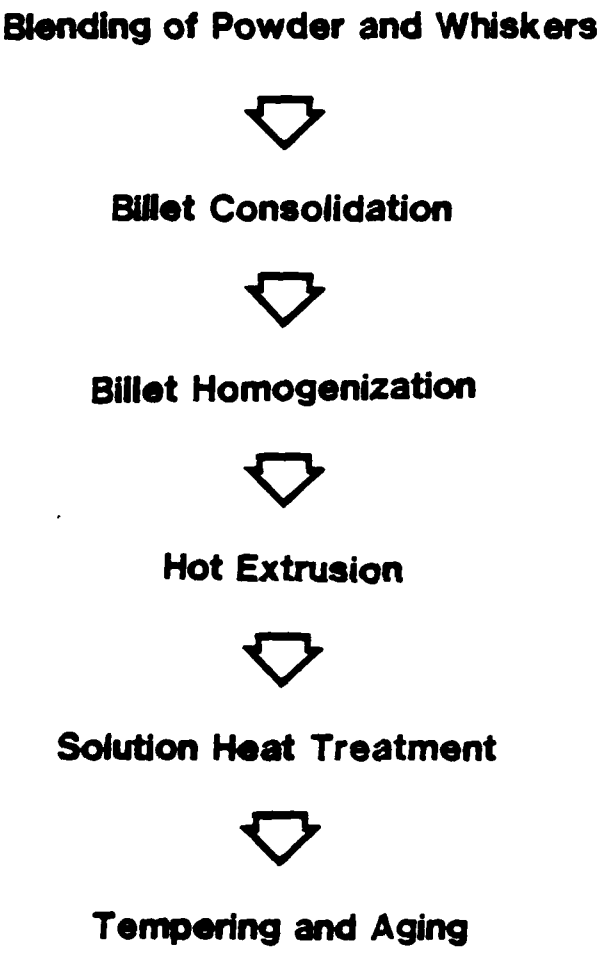

Figure 1. A typical flow chart depicting the production sequence for an extruded P/M metal matrix composite (5).

TABLE 2

HEAT TREATMENTS FOR P/M Al/SiC_w COMPOSITE AND MA-87 Al ALLOY

Material (Temper)	Solution Heat Treatment *	Aging
A(T6)	910°F, 1 hr	1. 4 days at R.T. 2. 24 hr at 250°F
B(T7)	910°F, 1 hr	1. 4 days at R.T. 2. 24 hr at 250°F 3. additional 14 hr at 350°F
C(T6)	A(T6) treatment plus 910°F, 2 hr	same as A(T6)
D(T6)	A(T6) treatment plus 950°F, 1 hr	same as A(T6)
E(T6)	A(T6) treatment plus 1050°F, 1 hr	same as A(T6)
F(T6)	A(T6) treatment plus repeating 910°F, 1 hr sequence twice	same as A(T6)
G(T6)	A(T6) treatment plus 950°F, 2 hr	same as A(T6)
MA-87	910°F, 2 hr plus stretched	1. 24 hr at 250°F 2. 4 hr at 325°F

*Treatment followed by water quenching

was employed. Preferential dissolution or initiation of pits during pre-exposure at open circuit potentials may have been the reasons for non-reproducibility in the former case. All electrochemical tests were performed with a PAR Model 351-2 Corrosion Measuring System.

MICROSTRUCTURAL STUDIES

All test specimens were examined after total immersion, potentiodynamic polarization, controlled-potential corrosion and galvanic-couple corrosion studies. Also, several specimens were examined after etching with Kellers reagent. The SEM and optical microscopes were used to observe preferential attack, SiCw orientation and distribution. The differential scanning calorimetric (DSC) technique was utilized to demonstrate any microscopic chemical differences between the skin and core regions of the A(T6) material.

ELEMENTAL ANALYSIS

Chemical analysis was performed on a number of samples taken from the skin and core regions of the A(T6) composite using the Inductively Coupled Plasma-atomic emission. All results were compared to the 7091Al alloy powder (see Table 1). Any deviation from this nominal composition would indicate the inhomogeneity of the composite.

HARDNESS MEASUREMENT

Knopp microhardness tests were made on the A(T6) material. For the Knopp test, the long edge of the diamond indenter was placed parallel to the direction of extrusion. All hardness measurements were done on the short transverse/longitudinal (S-L) face of both the skin and core regions of the same A(T6) specimen.

DENSITY MEASUREMENTS

The method for determining the void fraction and, therefore, the true density of the composite has been described by Schoutens (13). Briefly, the technique involves weighing specimens in air and in distilled water (T=25°C). For all density calculations, the SiCw distribution was assumed to be uniform throughout the skin and the core regions of the A(T6) material.

RESULTS AND DISCUSSION

CORROSION STUDIES

For the three-day total immersion test, the composite material, specimen A(T6), had the highest corrosion rate. The values for the composite in the 3.5% NaCl, pH 2 and pH 6 test solutions were 172.2 ± 44.0 and 18.6 ± 1.3 mdd, respectively; the corresponding values for the MA-87 alloy were 151.3 ± 8.1 and 13.6 ± 1.7 mdd, respectively. The high corrosion rate for the composite may be partially due to surface heterogeneity and partially resulting from the possible damage of SiCw during polishing. Mostly, it was observed that the skin of the A(T6) material corroded preferentially. Because of this preferential attack, the weight loss test data for the A(T6) specimen could not be properly compared with the MA-87 alloy.

A banded structure was observed on the A(T6) material during the total immersion test. A representative photograph of this banded structure is shown in Figure 2A. The circular marks near the edges and also middle of this sample were made by a Rockwell indenter before the sample was corroded. This banded structure was most probably due to processing problems such as billet fabrication, plate extrusion, the use of inhomogeneous prealloyed Al alloy powder, whisker impurities, machining or inadequate heat treatments. Elemental segregation resulting from inhomogeneous prealloyed powder or inadequate solution heat treatment may account for the observed preferential attack. Areas of differential etching on a SiCw/6061 Al alloy MMC have been reported and associated with either a difference in composition or internal strain energy (work hardening) (14). Some segregation of alloying constituents has been observed to occur during isothermal consolidation (vacuum hot pressing) of SiC/Al alloy MMC (6). For a P/M 2024 Al alloy the segregation of alloying elements has been minimized by applying longer homogenization times (15). A similar method may have to be applied to MMC. Longer solution heat treatment times or higher temperatures may be needed because conventional processes do not completely remove prior cold work history (16). Cocks and Brummer (17) have shown that residual stresses and severe crystallographic distortions due to specimen preparation (machining) caused the preferential corrosion attack of a 7075-T651 Al alloy. Preferential corrosion of an A(T6) material; which was machine-finished after heat treatment, was observed as shown in Figure 2B. The machine marks were identified after etching with dilute HCl. The effect of cold work on the corrosion behavior of an A(T6) specimen can be seen in Figure 2C. Here, the deformation was produced by a Rockwell B indenter. Note that the underlying plastic zone was preferentially attacked. Plastic deformation that may produce similar results can be produced by extrusion processes. When a billet is continuously extruded, zones of plastic deformation can extend to a larger fraction of the plate's cross section (18).

The effects of solution heat treatment on the exfoliation behavior of the A(T6) material were determined by varying treatment temperatures and times. Specimens C(T6) to G(T6) were immersed in aerated 3.5% NaCl, pH 2, solution. After the specimens were cleaned with 50 v/o nitric acid, faint banded structures were observed on the skin of each specimen, except for the G(T6) specimen. For specimens C(T6) to F(T6), the amount of preferential attack was less severe as compared to the A(T6) material. This is possibly an indication that the A(T6) material became less heterogeneous due to a reduction in internal strain energy during the subsequential solution heat treatments. The results of the exfoliation test for both the A(T6) and G(T6) specimens are shown in Figure 3. Figures 3A and 3B show the short transverse and the longitudinal faces of the specimens, respectively. In both the cases, however, the longitudinal faces showed Type ED (severe) exfoliation according to the ASTM standard (12). Apparently, the solution treatment did not improve the corrosion resistance of the longitudinal face, but it did show improvement for the short transverse face of the G(T6) specimen.

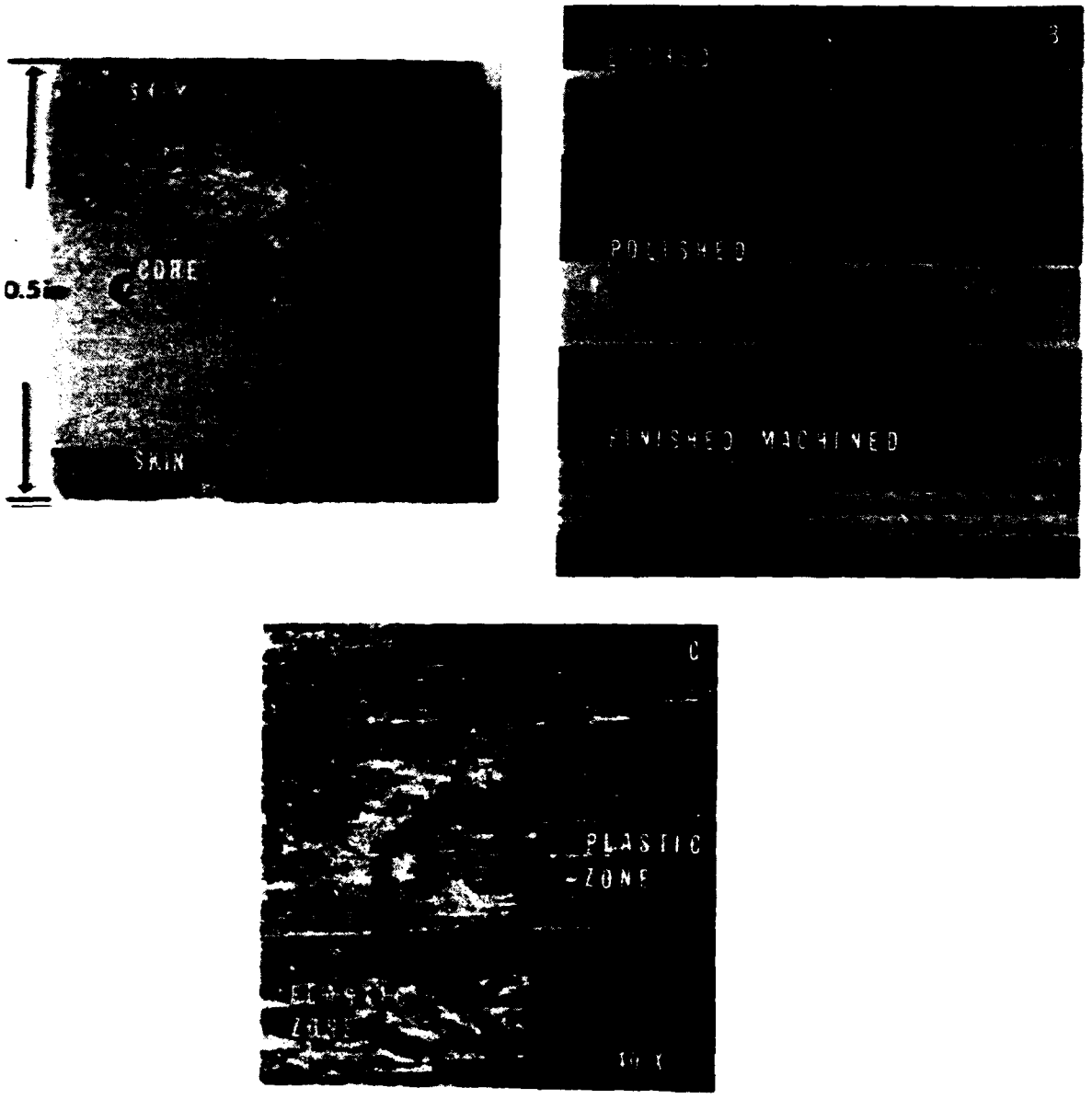

Figure 2. Photographs showing the preferential attack of the A(T6) P/M 7091 Al/SiCw composite in aerated 3.5% NaCl, pH 6. (A) specimen after total immersion for 3 days; (B) transverse face of a machine-finished specimen polished and etched showing residual work hardening effects; (C) Rockwell B indentation in the region with plastic zone corroded.

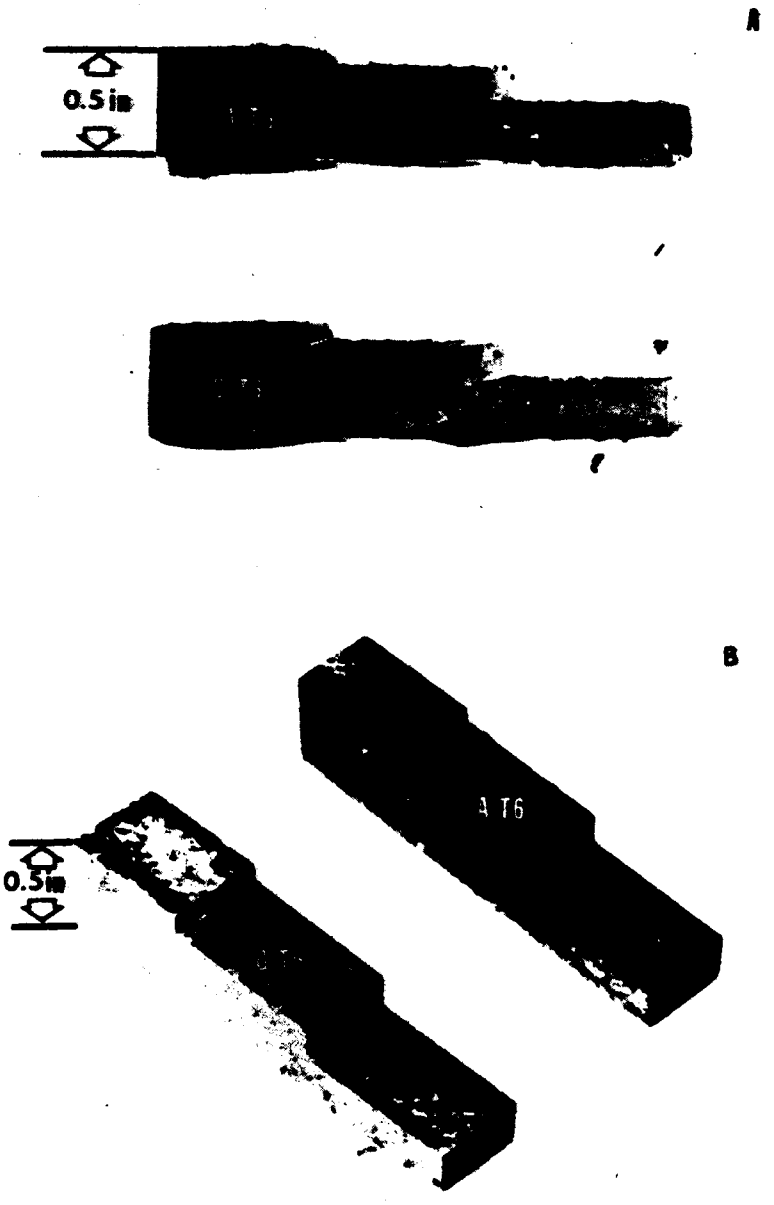

Figure 3. Exfoliation test specimens; (A) short transverse face, (B) short transverse and longitudinal faces.

ELECTROCHEMICAL STUDIES

Figure 4 shows the plots of galvanic current density, ig, versus time measurements for couples made of material A(T6) and MA-87 alloy (Couple A), and between the skin and core of the A(T6) material (Couple B). It was observed that for couple (A), the MA-87 was always anodic to the A(T6) specimen and the ig increased with time (Figure 4, curve A). For couple (B), the skin remained anodic to the core and showed increasing ig with time (Figure 4, curve B). The addition of SiCw to the Al alloy matrix may have shifted the corrosion potential to more positive potentials for the A(T6) specimen. This effect was observed by Trzaskoma and McCafferty (9). Optical micrographs of the test specimens show that the grain boundaries of the MA-87 specimen were etched and the A(T6) specimen revealed a few exposed SiCw. In the case of couple B (Figure 4), the core was more noble than the skin region of the A(T6) specimen. Optical micrographs of the test specimens show that the Al alloy rich zones in the skin region were completely etched out whereas the core did have a few pits and exposed SiCw.

The corrosion potential versus time curves are given in Figure 5 for the A(T6) material, its core and skin regions and the MA-87 alloy in a deaerated 3.5% NaCl, pH 6, solution. As shown, initially the potential decreased rapidly with time to -0.810 V for the core and to approximately -1.10 V for the A(T6) and MA-87 alloy. For the skin region, the potential started from approximately -1.20 volts. The higher negative potential may be due to zinc either in solid solution with Al or segregated in the skin (19). Except for the skin region, the E (corr) vs. time curves generally showed a minimum and then returned to a more positive value. The steady-state corrosion potential for the MA-87 alloy was the most negative (anodic). The less active potential for the core region may reflect high packing density for SiCw in that region (9).

The potentiodynamic polarization behavior for the skin and the core region of the A(T6) material and A(T6) as a whole are given in Figure 6. These results were obtained by starting the polarization scan as soon as the test specimen was immersed in the test solution. Typical polarization test results, obtained after corrosion potential and polarization resistance tests were run, are given in Table 3. The reproducibility of the polarization curves was greatly influenced by the thickness of the skin region, segregation of matrix alloying constituents, SiCw, Al alloy matrix-rich zones and workhardening resulting from sample preparation. Since polarization test specimens were cut from used mechanical test specimens, residual stresses or workhardening from machining may have affected these results. Also, voids on the surface may have been an important factor since these can change into large pits due to corrosion. Cathodically protecting the test specimen before the start of the polarization scan (i.e. at -1.2 V) may have decreased the number of pits and crevices formed during the corrosion potential measurements, thus improving reproducibility of the results. As shown in Figure 6, the polarization plots do reflect the more noble characteristics of the core region. The more positive E(I=0) value for the core region (see Figure 6) may be possibly due to a more positive dissolution potential because of the grain orientation (17, 20, 21, 22) or a higher concentration of copper (23). As shown in Table 3, the skin region of the A(T6) specimen has a slightly larger cathodic tafel slope. This indicates that it is harder to evolve hydrogen gas on the skin region; it is probably because the skin region may contain a smaller amount of copper. Doig and Flewilt (24), and Peel and Poole (25) have studied various solid solutions of Al-Zn-Mg-Cu alloys in 3.5% NaCl, pH 6. They have shown that increasing the copper concentration in solid solution in these alloys displaces the polarization curves to higher current densities while zinc and magnesium concentration variations in solid solution have no effect. A similar explanation may be given for the effects observed on the A(T6) specimen where the preferential corrosion of the skin region occurred.

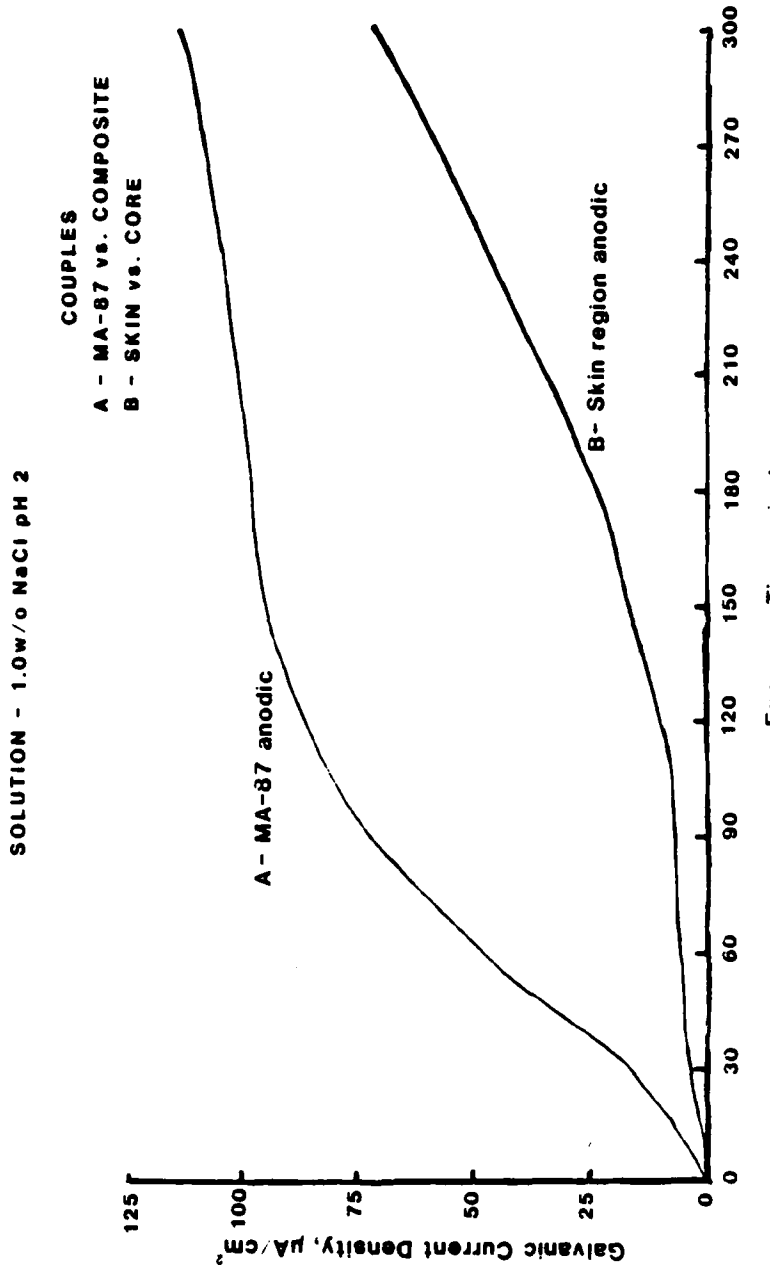

Figure 4. Galvanic current density/time plots of (A) A(T6) specimen versus MA-87 alloy and (B) skin versus core regions of A(T6) specimen in aerated 1.0% NaCl, pH 2.

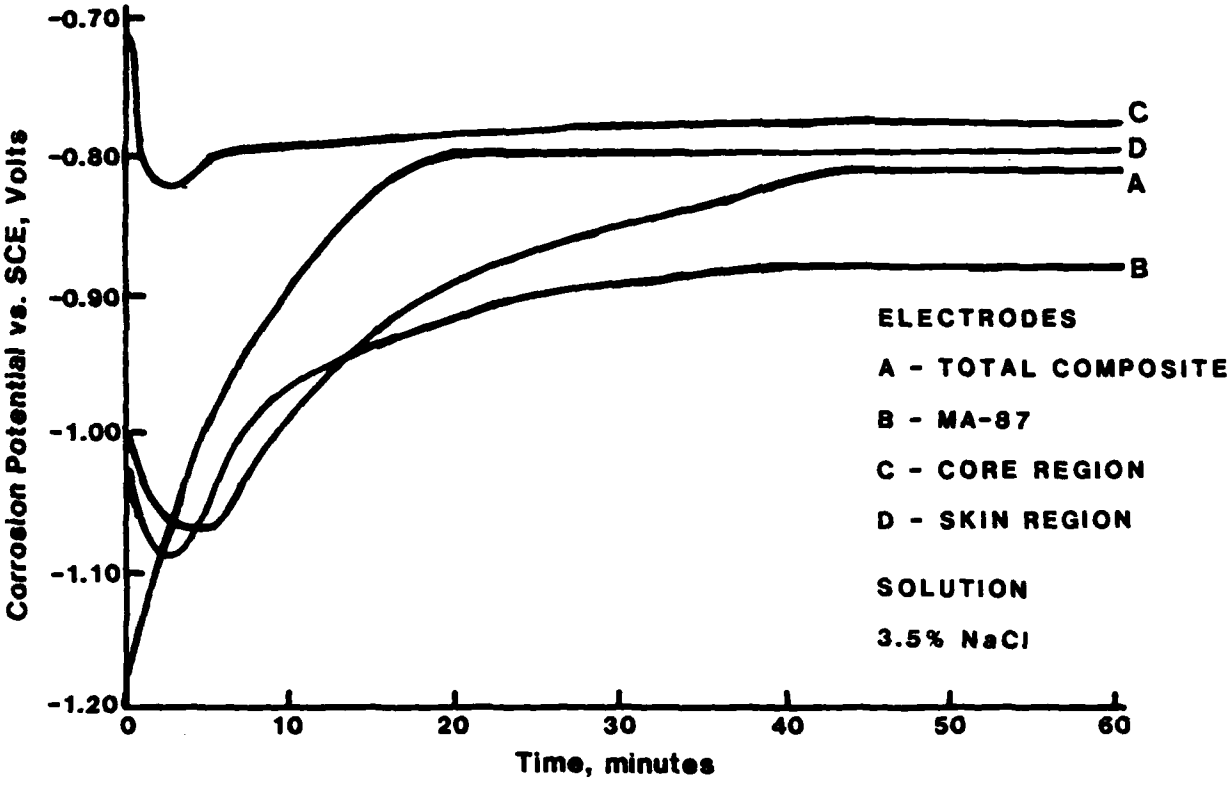

Figure 5. Corrosion potential versus time plots for; (A) A(T6) (B) MA-87, (C) and (D), the core and skin regions of the A(T6) in deaerated 3.5% NaCl, pH 6.

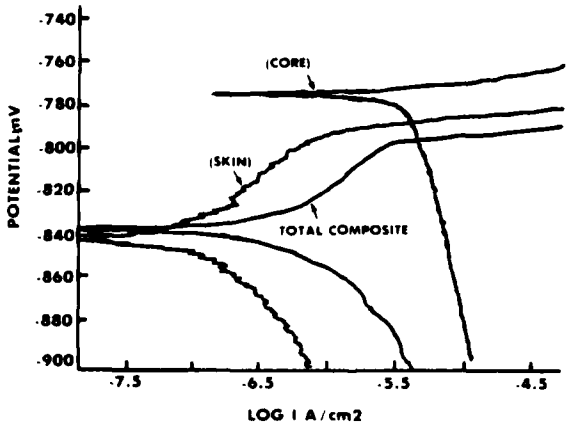

Figure 6. Potentiodynamic polarization behavior of the composite: (A) A(T6) specimen, (B) skin and (C) core regions of specimen A(T6) in deaerated 3.5% NaCl, pH 6.

TABLE 3

TYPICAL CORROSION POTENTIAL, POLARIZATION RESISTANCE AND POTENTIODYNAMIC TEST RESULTS

Electrochemical Parameters	Specimen			
	A(T6) composite (skin and core regions)	A(T6) composite Core	A(T6) composite Skin	MA-87
E_{oc}, V	-0.804	-0.782	-0.803	-0.880
R_p, Ohms	12.8×10^3	21.9×10^3	13.5×10^3	50.4×10^3
E(Is0), V	-0.838	-0.811	-0.800	-0.982
R_p, Ohms	20×10^3	38×10^3	2.76×10^3	11.5×10^3
β_c, V/dec	0.174	0.177	0.196	0.129
β_a, V/dec	0.075	0.100	0.099	0.090
I_{corr}, A/cm^2	8.59×10^{-7}	7.0×10^{-7}	2×10^{-6}	6×10^{-7}

The effect of potential on the A(T6) material, was determined by applying a constant potential where the skin region on the same specimen was observed to preferentially corrode. A 3.5% NaCl, pH 6, deaerated solution was used and a potential of -0.69 V was applied for a period of three hours. Figure 7A shows the skin region before the start of the test. Figures 7B and 7C are the photographs after the test showing that the skin region's matrix material was mostly removed and the core region remained bright and mostly unattacked, with a few pits. It is to be noted that similar tests done in other electrolytes, without chloride ions, did not produce the banded structure. Also, if the constant applied potential was shifted to more positive potentials in the deaerated 3.5% NaCl (pH 6) solution, the core region's matrix material was also dissolved. In other words the dissolution potential of the core region was less active than skin.

SCANNING ELECTRON AND OPTICAL MICROSCOPY

The A(T6) material's skin and core regions were further examined using the scanning electron and optical microscopes. A scanning electron micrograph of the A(T6) specimen's core region polished to 0.05 μm alumina and etched with Kellers reagent is shown in Figure 8. Generally, the amount of Al alloy matrix and SiCw rich zones in the core region were not as large as the skin region. In both the core and skin regions large black SiC particles ranging in diameter from 5 to 10 microns were observed. But, foreign particles (Figure 9) were discovered only in the skin region of the composite.

Figure 10 shows scanning electron micrographs of the skin and core regions of the A(T6) material after total immersion in aerated 3.5% NaCl, pH 2. The micrographs of the skin region (Figures 10 A and B) show that a larger amount of the Al alloy-rich zones had been dissolved with some of the matrix material adhering to the whiskers. The Al alloy matrix material on the SiCw may have been the result of the extrusion process. A temperature increase of the extruding plate, which may result from the friction between the plate and the die can cause partial melting of the skin region of the composite (26). Thus a less active phase may have possibly precipitated at the SiCw/Al alloy interface. The micrographs of the core region (Figures 10 C and D) show the absence of matrix material at the SiCw-matrix interface region. The selective dissolution may be due to the crystallographic orientation or the recrystallization of the grains in the core region. Since the SiCw/Al alloy composite matrix material contains SiCw and/or SiC particles, the flow patterns of the composite material during the extrusion process may be different than extrusions of materials without reinforcement. Thus, during the extrusion of the composite, the core region may have became highly cold worked and, as a result, recrystallized. Electrochemical potential differences can exist between the recrystallized and unrecrystallized grain structures of extrusions of high strength alloys. The large recrystallized grains are slightly cathodic (by approximately 20 mv) to the unrecrystallized grain structure (27).

Figures 11A and 11B show the optical micrographs of the microstructure of the skin and core regions, respectively, of the A(T6) material which were revealed after total immersion in aerated 1% NaCl, pH 6 for three hours. The large grains in the core region (Figure 11B) as compared to those in the skin region are due to the large prealloyed powder particles which were not stringed like those in the skin region. The grain size of the matrix may have an effect on the corrosion susceptibility of the composite since a larger number of grains per unit area of the composite contains a larger number of grain boundary precipitates. It was observed from the optical micrograph (Figure 11A) that the skin region contains a considerable number of smaller grains than the core region (Figure 11B) of the MMC and therefore a larger number of grain boundary precipitates. Generally, in the skin region of the specimen, the microstructure appeared to by crystallographically oriented and cubic in shape (Figure 11A). The core region of the same specimen (Figure 11B) did not show any preferential orientation or general shape. A representative optical micrograph of the core

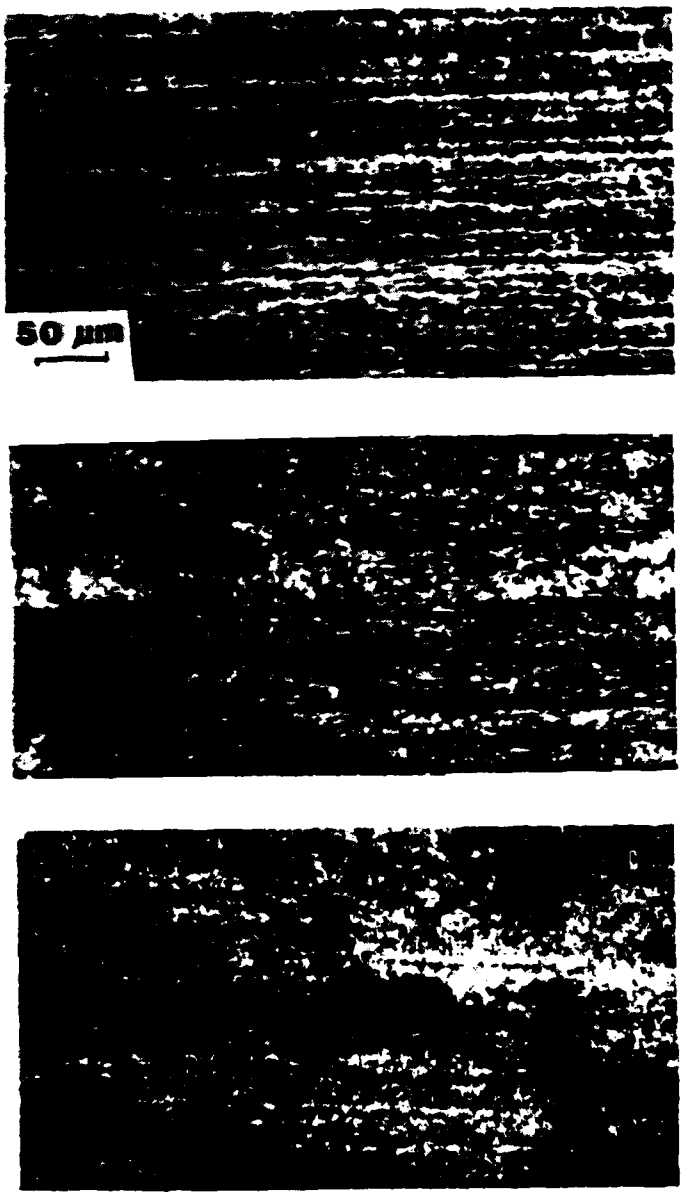

Figure 7. Optical micrographs of the A(T6) specimen's (A) skin region before testing, (B) skin region and (C) core region after polarization at -0.69V. Magnification 200x.

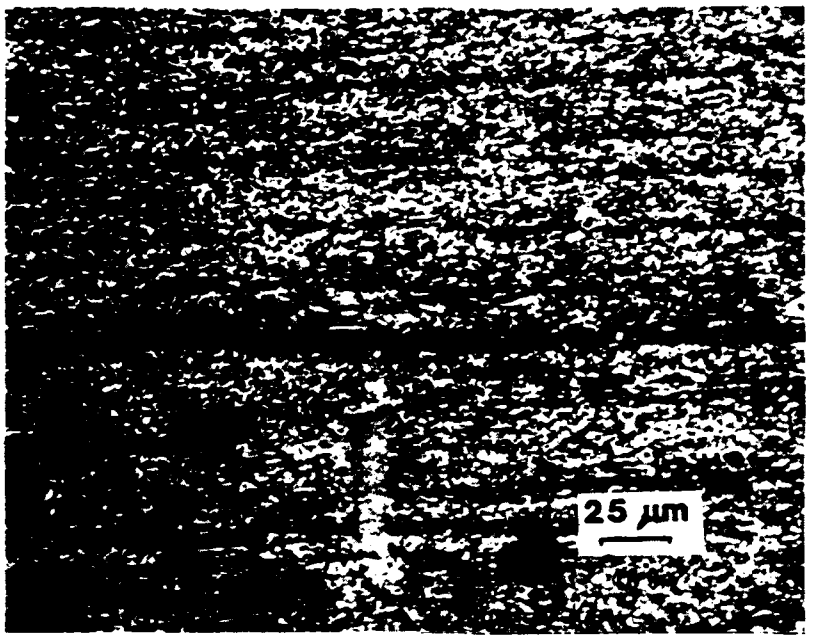

Figure 8. Scanning electron micrograph of the A(T6) specimen's core region etched with Kellers reagent. Magnification 400x.

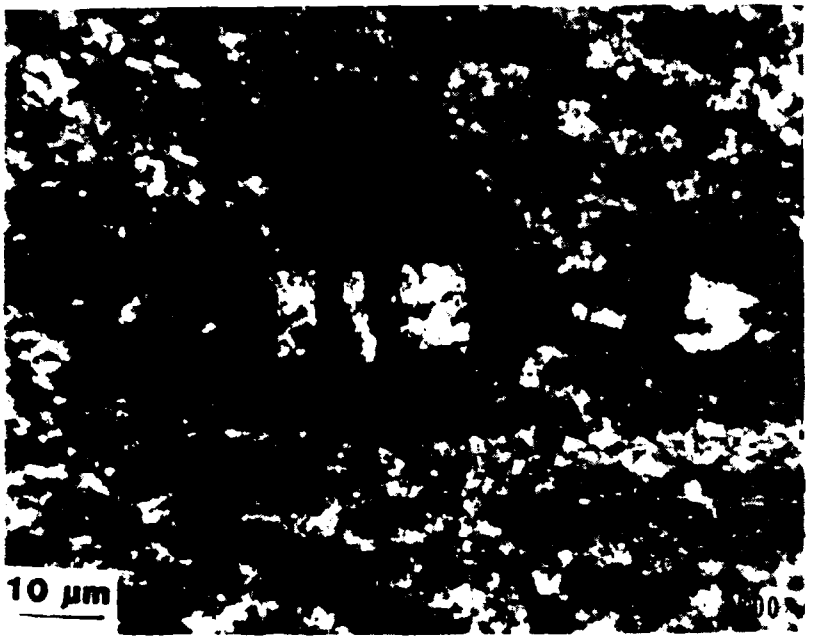

Figure 9. Optical micrograph of the A(T6) specimen's skin region etched with Kellers reagent showing foreign particles not broken-up by the extrusion process. Magnification 800x.

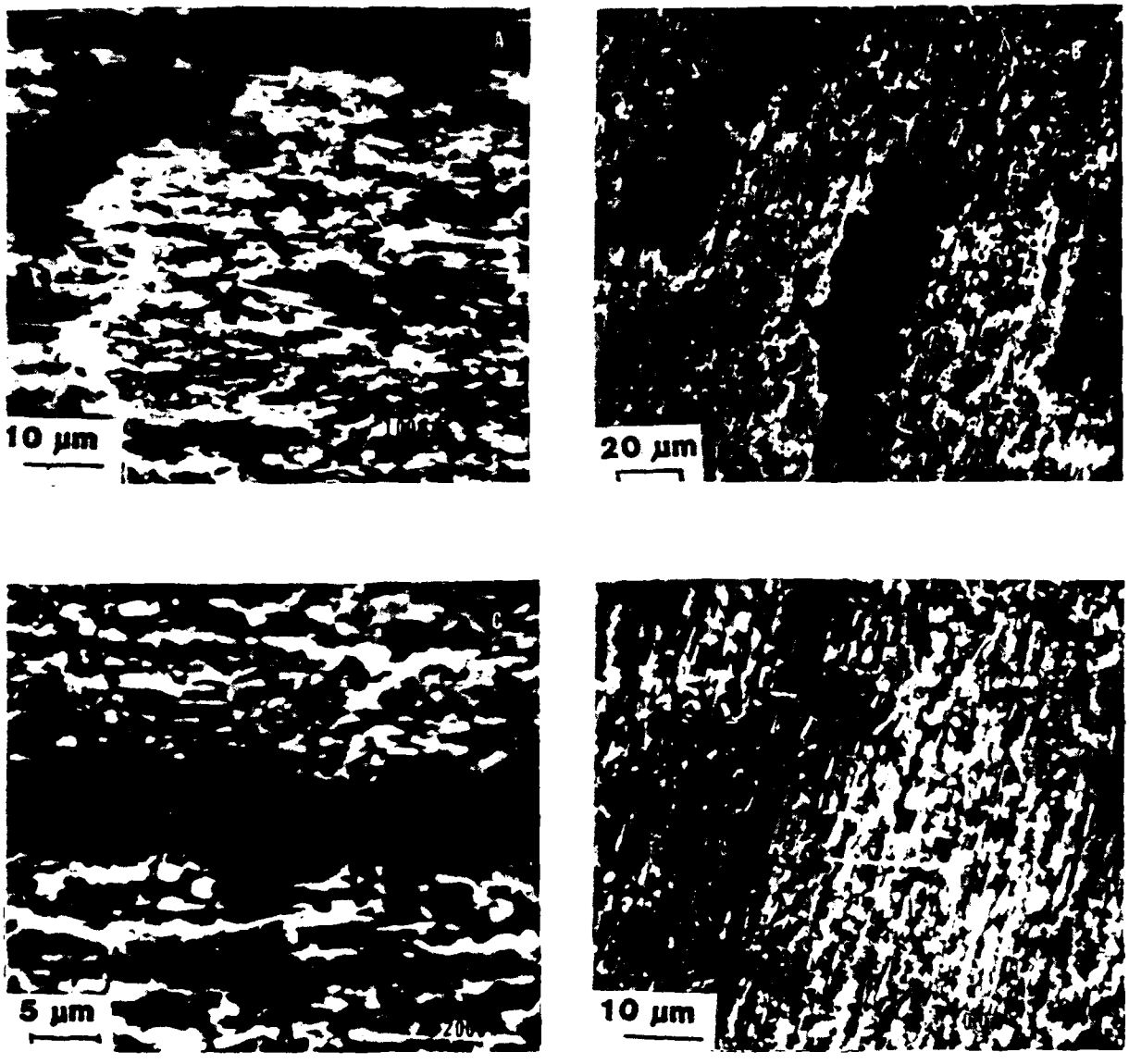

Figure 10. Scanning electron micrographs of the A(T6) specimen's skin region at (A) 1000x and (B) 520x; and core region at (C) 2000x and (D) 1000x after the total immersion in aerated 3.5% NaCl, pH 2.

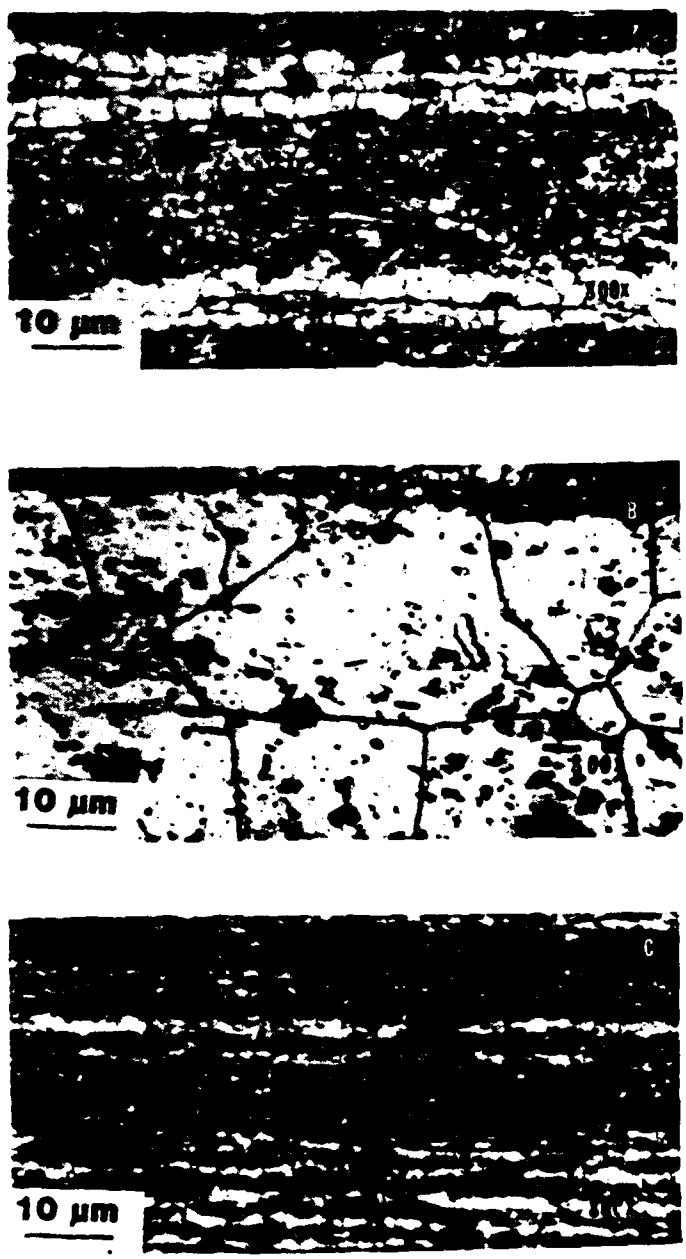

Figure 11. Optical micrographs of the A(T6) specimen's (A) skin region, (B) core region; and (C) core region of the G(T6) specimen after total immersion in aerated 1% NaCl, pH 6 for three hours. Magnification 800x.

region appears to be similar in microstructure to that of the skin regions of the A(T6) and G(T6) materials. This possibly indicates that the A(T6) material may have become completely homogenized. This may be the reason why the core region of the short transverse face of the G&T6) specimen was more resistant to corrosion than the A(T6) specimen in the exfoliation tests (cf. Figure 3B).

EDAX, DSC AND X-RAY ANALYSIS

An A(T6) specimen was electrochemically etched for 10 minutes at a potential of -0.69V in 1% NaCl, pH 2 to perform EDAX analysis. The A(T6) specimen was cleaned in 50 v/o nitric acid to remove any corrosion products. Figure 12A shows a scanning electron micrograph of the specimen after testing. Figures 12B and 12C are the elemental X-ray maps for zinc and copper, respectively, for the area shown in Figure 12A. As shown, the smoother region in the micrograph (Figure 12A) is zinc rich surrounded by copper rich areas. At the applied potential of -0.69V the copper-rich areas of the specimen are cathodic. Therefore they should be protected, whereas zinc, which is anodic, will undergo dissolution.

Differential scanning calorimetry was employed to identify the phases (precipitates) and possible differences that may exist between the skin and core regions of the A(T6) material. Samples tested indicated no major differences between the two regions. Major precipitate phases or any variation in their concentrations can possibly be masked by the presence of the whiskers, since the thermal conductivity of the SiCw is vastly different than that of the Al alloy matrix. It should be noted that the preferential orientation of the grains, segregation of alloying elements and/or void content (porosity) could not be observed during these tests.

X-ray diffraction studies were done on both the skin and core regions of the same A(T6) specimen. Results have indicated that there were no major differences in structure or phases between the skin and core regions of the specimen. Both the Al and beta-SiCw peaks were observed. The beta-SiCw peaks for the skin region were lower in intensity than for the core region of the same specimen indicating a possibility of a lower concentration of SiCw in the skin region. Also, for each region of the A(T6) specimen, the maximum intensity peak for Al was at $2\theta^\circ = 65.2^\circ$ as opposed to $2\theta^\circ = 44.7^\circ$, which possibly indicates preferred orientation of the grains. Other minor observed peaks could not be identified, but they were determined not to be aluminum carbide. Active dispersoids such as aluminum carbide may be formed from trapped hydrocarbons when the composite is subjected to high temperature e.g. above 500°C (27). Such a temperature could be reached readily during the extrusion process.

ELEMENTAL ANALYSIS

Both the skin and core regions of the A(T6) material were analyzed to observe any variations in the composition. Due to the heterogeneity of the composite, reproducible results could not be obtained. This was exacerbated due to the use of small sample sizes, e.g., less than 100 mg. Typical results of the chemical analysis are listed in Table 1. Abnormally high iron concentrations in the skin and core regions of the A(T6) material were observed and, for all test runs, the skin region contained a larger concentration of iron. This may account for the preferential corrosion of the skin layer. The high iron concentration observed in the skin regions of the A(T6) material may be due to impurities from the SiCw (28, 29) or related to the extrusion container die. Prealloyed Al powder chemical analysis (Table 2) did not show the high iron concentration. Generally, it was observed from the analyses that the core region specimen had higher copper, silicon, and cobalt concentrations. The higher zinc and copper concentrations were observed from the EDAX analysis, and possibly had an effect on the potentiodynamic polarization plots of the skin and core regions

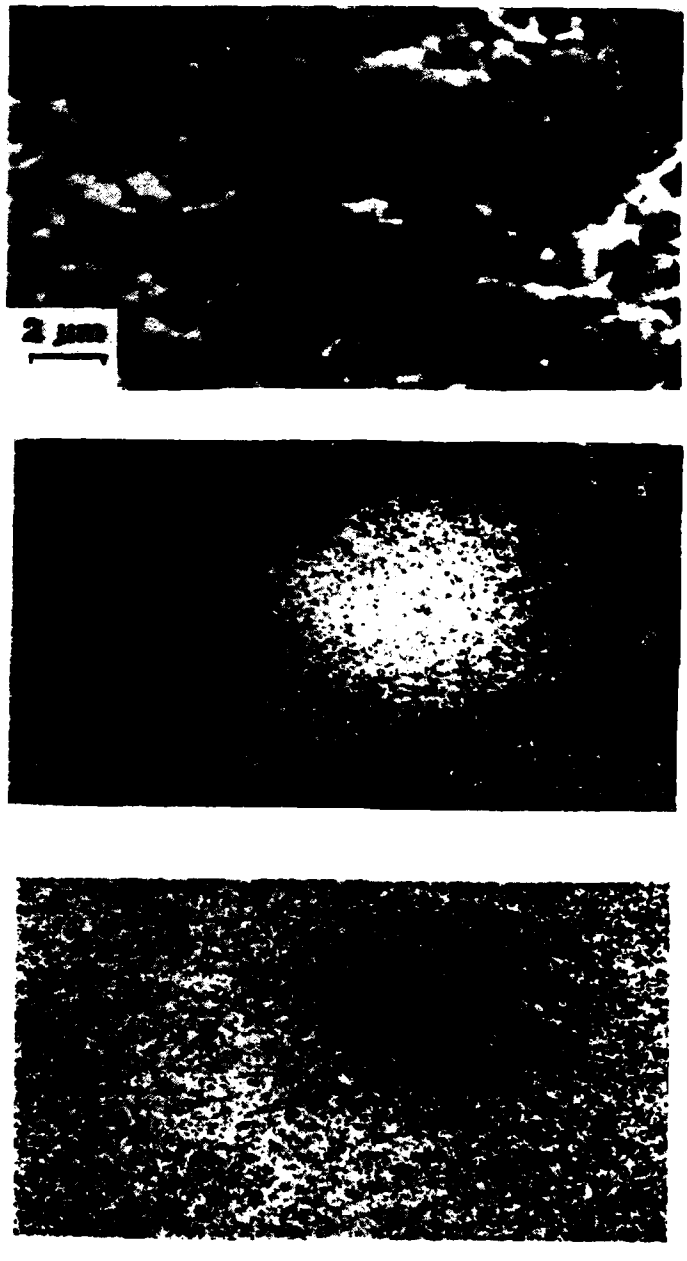

Figure 12. (A) Scanning electron micrograph of the A(T6) specimen electrochemically etched at -0.69V in deaerated 1% NaCl, pH 2 for 10 minutes; (B) and (C) are the X-ray mappings for zinc and copper, respectively, for figure (A). Magnification 5000x.

of the A(T6) material. The skin region with higher iron concentrations also had a larger magnesium concentration. High concentrations of calcium and silicon were found on a number of skin and core specimens. Although elemental segregation can account for pitting or localized corrosion it can not be the sole reason for general dissolution of the matrix material in the skin region. This has been shown in Figure 2A, where the line of separation between the skin and core regions was well marked.

HARDNESS TESTS

The results of the Knoop microhardness tests are shown in Figure 13, and indicate that the skin region is softer than the core region. The Knoop microhardness values increased as the distance from the edge of the specimen increased (up to 0.10 in. thickness) whereas the core material hardness remained almost constant (Figure 13). The lower may be the result of Al alloy-rich zones as shown in Figure 7A. The Al rich zones would be softer since there is no SiCw reinforcement present. The high void content of the SiCw/Al alloy composite of both the skin and core regions may also lower the hardness values than normally would be observed in a composite without voids.

DENSITY MEASUREMENTS

Figures 14A and 14B show scanning electron micrographs of the skin and core regions, respectively, of an A(T6) specimen polished down to 0.05 μm alumina. As can be seen, there is a higher void (appearing as black spots) concentration on the surface of the skin region as compared to the core region. Density measurements were made to determine if the high porosity of the polished specimens may be due to whisker pull-out during polishing. Samples weighing 0.25 gram for the skin and 0.18 gram for the core regions were taken and polished to 0.05 μm alumina. The density of the whole A(T6) material was calculated to be 3.096 g/cc. The average values for the density of the skin and core regions were determined to be 2.788 $\pm$ 0.102 and 2.803 $\pm$ 0.121 g/cc, respectively. This corresponds to a density difference or void fraction of 10.27 $\pm$ 3.0% and 9.53 $\pm$ 3.93% between the calculated value for the material and the skin and core, respectively. The percent difference or void fraction values are surprisingly high and may not indicate the total void fraction of the skin and core. This may be partly due to experimental limitations given by Schoutens (13). However, the results do indicate that there are variations in the density throughout the composite. Earlier billets of SiCw/Al alloy composites manufactured by Arco Metals Co. contained a high void content (30). This problem was associated with improper outgassing and heating times. A similar processing problem was observed by Pinkerton (31) in the manufacturing of PM 2024 Al alloy. Large bubble-like protrusions on the surface of this alloy were observed after heating. Apparently, these protrusions were due to entrapped gas which expanded and formed large voids during high temperature processing. A similar observation was made during the solution heat treatment of the A(T6) material at 1075°F. The protrusions were mostly concentrated on the skin of the A(T6) material and coincided with the banded structure as shown in Figure 2A.

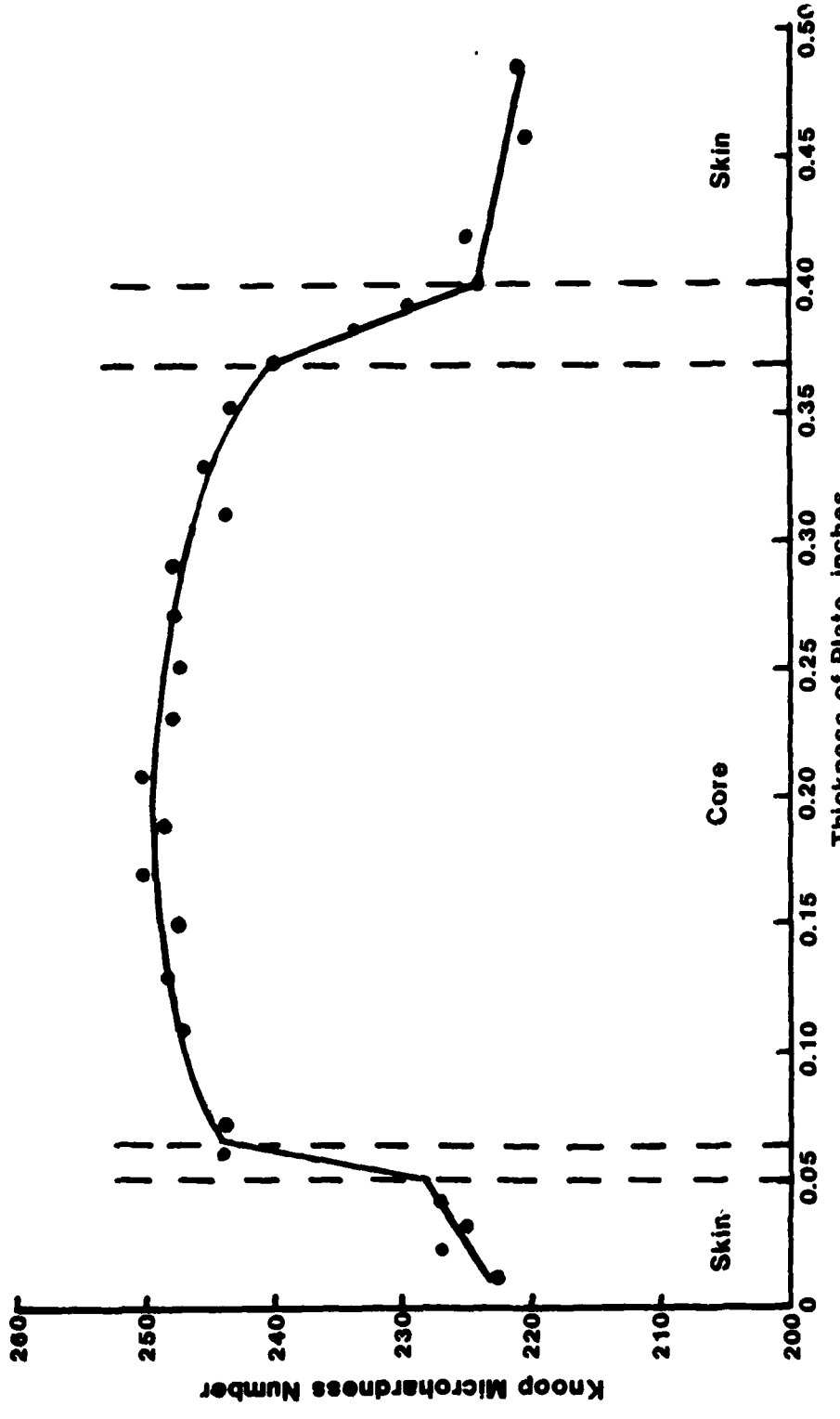

Figure 13. Profile of the Knoop microhardness values across the composite plate thickness.

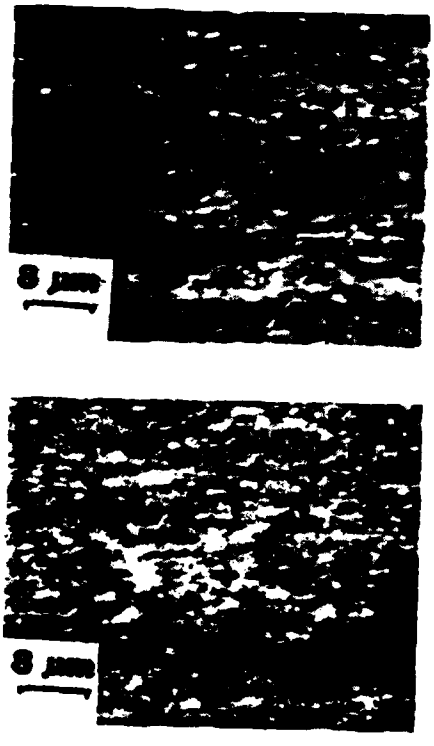

Figure 14. Scanning electron micrographs of the A(T6) specimen's (A) skin and (B) core regions. Final polished to 0.05 μm Al_2O_3. Magnification 1200x.

CONCLUSIONS

The role of processing on the corrosion susceptibility of a P/M 7091Al alloy 20v/o SiCw composite was studied. It was found that the composite plate exhibited an abnormal corrosion behavior. The composite plate's exterior (skin areas) was observed to preferentially corrode in chloride solutions. The banded structure observed on the SiCw/Al alloy composite in the T6 and T7 conditions was determined to be associated with processing. Based on this work, the following conclusions were made:

1. The fabrication of prealloyed 7091Al powder and the composite's processing parameters may have caused constituent segregation and a high porosity in the material. It was observed that the skin region contained a higher void fraction and a higher iron concentration as compared to the core, whereas the core region contained a higher copper concentration. The composite also contained Al and SiCw rich zones.

2. The extrusion process and/or specimen machining may have introduced plastic deformation (workhardening) or recrystallization of portions of the composite. Conventional solution heat treatments may have not relieved prior cold work history. It was observed that substantial solution heat treatment at 950°F for two hours eliminated the preferential attack of the skin of the composite. The material may have become homogenized and/or the residual stresses may have been relieved.

On the basis of the above, processing variables must be rigidly controlled or else the corrosion properties of metal matrix composites may be drastically altered.

REFERENCES

1. M. Metzger, S.G. Fishman, Ind. Eng. Chem. Prod. Res. Dev., Vol. 22, No. 2, pp. 296-302 (1983).

2. E.L. Thellmann, B.E. Sandman, W.C. Harrigan Jr., "Application of Powdered-Base Metal Matrix Composites to Torpedoes," Naval Underwater Systems Center, Contract #N00140-80-G-9905-0002, Feb. 1981.

3. D.L. McDanels, "Analysis of Stress-Strain, Fracture and Ductility Behavior of Aluminum Matrix Composites Containing Discontinuous Silicon Carbide Reinforcement," NASA Technical Memorandum 83610, p. 7, March 1984.

4. T.G. Nieh, R.F. Karlak, J. Mater. Sci. Let., No. 2, pp. 119-122 (1983).

5. A.P. Divecha, S.G. Fishman, S.D. Karmarkar, J. Metals No. 9, pp. 12-17 (1981).

6. J.E. Schoutens, "Discontinuous Silicon Carbide Reinforced Aluminum Metal Matrix Composites Data Review," MMCIAC Databook Series MMCIAC No. 000461, p. 9-17, Dec. (1984).

7. D.L. McDanels, op. cit., p. 8.

8. J.E. Schoutens in ref 6 p. 5-217.

9. P.P. Trzaskoma, E. McCafferty, J. Electrochem. Soc., Vol. 130, No. 9, pp. 1804-1809 (1984).

10. D. Aylor, P.J. Moran, "Effect of Reinforcement on the Pitting Behavior of Aluminum-Base Metal Matrix Composites," David W. Taylor Naval Ship And Development Center/Ship Materials Engineering 85/42, July (1985).

11. K.D. Lore, J.S. Wolf, "Extended Abstracts," The Electrochemical Society Denver Meeting Oct. 1981, The Electrochemical Society, Princeton, NJ, 1981, Abstr. 154.

12. Metals Corrosion Erosion, and Wear, "Exfoliation Corrosion Susceptibility in 2xxx and 7xxx Series Aluminum Alloys (EXCO TEST)," 1984 Annual Book of ASTM Standards, Vol. 0302, Philadelphia, Pa. 19103.

13. J.E. Schoutens, J. Mater. Sci., Vol. 19, pp. 957-964 (1984).

14. D.L. McDanels op. cit. 3, p. 2.

15. J.E. Schoutens in ref 6, p. 5-194.

16. J.E. Schoutens in ref 6, p. 5-103.

17. F.H. Cocks, S.B. Brummer in Proceedings 4th International Congress on Metallic Corrosion, Ed. N.E. Hummer, pp. 58-64 (1972).

18. K. Laue, H. Stenger, Extrusions, ASM Metals Parks, Ohio (1976), p. 19.

19. W.W. Binger, E.H. Hollingsworth, D.O. Sprowls in Al-Properties; Physical Metallurgy and Phase Diagrams, Vol. I, ASM, p. 213 (1967).

20. J.E. Hatch, Ed., Aluminum; Properties and Physical Metallurgy ASM, Metals Park Ohio (1984) p. 281.

21. A.H. Roebuck, J.V. Luhan, Corrosion, Vol. 23, No. 9, pp. 268-275 (1962).

22. B.W. Lifka, D.O. Sprowls, J.G. Kaufman, Corrosion, Vol. 23, No. 11, pp. 335-342 (1967).

23. W.W. Binger, E.H. Hollingsworth, D.O. Sprowls, op. cit., p. 228.

24. P. Doig, P.E.J. Flewilt, J.W. Edington, Corrosion, Vol. 33, No. 6, pp. 217-221 (1977).

25. C.J. Peel, P. Poole in Mechanisms of Environment Sensitive Cracking of Materials, P.R. Swann, F.P. Ford, Eds., The Metals Society, p. 147 (1977).

26. J.E. Schoutens in ref 6, p. 9-22.

27. W.W. Binger, E.H. Hollingsworth, D.O. Sprowls in ref 21, p. 217.

28. P.S. Gilman, W.D. Dix, Metall. Trans. Vol. 12A, No. 5, pp. 813-824 (1981).

29. J.E. Schoutens in ref 6, p. 2-11.

30. C.H. Anderson, R. Warren, Composites, Vol. 15, No. 1, pp. 16-24 (1984).

31. J.E. Schoutens in ref 6, p. 9-6.

DISTRIBUTION LIST (Continued)

	No. of Copies
Wright-Patterson Air Force Base WPAFB (AFWAL/MLSA) OH 45433 (Mr. B. Cohen)	1
Air Force Logistics Center (MMEMC) Warner-Robbins AFB Warner, GA 31098 (Mr. W. Thompson)	1
Army Research Office P.O. Box 12211 Research Triangle Park; NC 27709 (Dr. R. Reeber)	1
U.S. Army Materials and Mechanics Research Center (DRXMR-EM), Watertown, MA 02172 (Dr. M. Levy)	1
U.S. Army Armament R&D Command (DRDAR-SCM) Bldg. 355, Dover, NJ 07801	1
U.S. Army Mobility Equipment R&D Command (DRDME-VC) Fort Belvoir, VA 22060 (Mr. D.A. Emeric)	1
National Bureau of Standards Washington, DC 20234	1
Dr. H. Leidheiser, Jr Center for Coatings and Surface Research Lehigh University Bethlehem, PA 18015	1
Dr. M. Kendig Rockwell International Science Center 1049 Camino Dos Rios, P.O. Box 1085 Thousand Oaks, CA 91360	1
Dr. C. McMahon, LRSM University of Pennsylvania Philadelphia, PA 19104	1
Defense Technical Information Center Attn. DTIC-DDA-1 Cameron Station, Bldg. 5 Alexandria, VA 22314	12
NAVAIRDEVCEN (3 for Code 8131) (50 for Code 6062, V. Agarwala)	53

DISTRIBUTION LIST (Continued)

	No. of Copies
Commander..... Naval Air Force U.S. Pacific Fleet Attn: Code 7412 San Diego, CA 92135	1
Naval Sea Systems Command ..... Washington, DC 20362	1
Chief of Naval Material ..... Navy Department Washington, DC 20350	1
Office of Naval Research..... 800 N. Quincy St. Arlington, VA 22217 (Dr. A.J. Sedriks)	1
Office of Naval Technology..... NAVMAT-0725 800 N. Quincy St. Arlington, VA 22217 (Mr. J.J. Kelly)	1
Naval Research Laboratory..... 4555 Overlook Ave. Washington, DC 20375 (Mr. J. Good)	1
David Taylor Ship Research Development Center..... Code (281) Annapolis, MD 21402 (Mr. A.G.S. Morton, Mr. G. Wacker)	2
Naval Surface Weapons Center (Code R-30) ..... White Oak Silver Springs, MD 20910	1
Naval Air Propulsion Center (Code PE-72) ..... Trenton, NJ 08628 (Mr. A.J. Dorazio)	1
Naval Underwater Systems Center (Code 4493) ..... New London, CT 06320 (Dr. R.G. Kasper)	1
Air Force Office of Scientific Research, Bolling Air Force Base ..... Washington, DC 20332 (Dr. A. Rosenstein)	1

DISTRIBUTION LIST

	No. of Copies
Naval Air Systems Command (2 for AIR-7226) (1 for AIR-31A) (2 for AIR-5304) (1 for AIR-5142) (1 for AIR-03D)	6
Commanding Officer Naval Air Rework Facility Attn: Code (340) Naval Air Station Alameda, CA 94501	1
Commanding Officer Naval Air Rework Facility Attn: Code (340) Naval Air Station Jacksonville, FL 32212	1
Commanding Officer Naval Air Rework Facility Attn: Code (340) Naval Air Station Norfolk, VA 23511	1
Commanding Officer Naval Air Rework Facility Attn: Code (340) Naval Air Station North Island San Diego, CA 92135	1
Commanding Officer Naval Air Rework Facility Attn: Code (340) Naval Air Station Pensacola, FL 32508	1
Commanding Officer Naval Air Rework Facility Attn: Code (340) Marine Corp. Air Station Cherry Point, NC 28533	1
Commander Naval Air Force U.S. Atlantic Fleet Attn: Code 5281 Norfolk, VA 23511	1

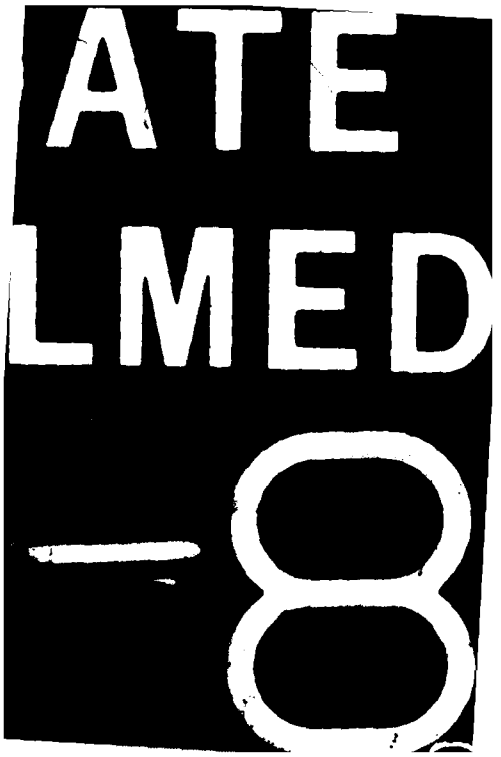
ATE
LMED
8